

Hip Fracture Risk Assessment in Elderly and Diabetic Patients: Combining Autonomous Finite Element Analysis and Machine Learning

Zohar Yosibash,^{1,2} Nir Trabelsi,^{2,3} Itay Buchnik,⁴ Kent W Myers,³ Moshe Salai,⁵ Iris Eshed,^{6,7} Yiftach Barash,^{6,7} Eyal Klang,^{6,7} and Liana Tripto-Shkolnik^{7,8}

¹School of Mechanical Engineering, The Iby and Aladar Fleischman Faculty of Engineering, Tel Aviv University, Tel Aviv, Israel

²PerSimiO Ltd, Beer-Sheva, Israel

³Department of Mechanical Engineering, Shamoon College of Engineering, Beer-Sheva, Israel

⁴Department of Electrical and Computer Engineering, Ben Gurion University, Beer-Sheva, Israel

⁵Orthopedic Department, Tel Aviv Sourasky Medical Center, Tel Aviv, Israel

⁶Department of Diagnostic Imaging, Sheba Medical Center, Tel Hashomer, Israel

⁷Sackler School of Medicine, Tel Aviv University, Tel Aviv, Israel

⁸Division of Endocrinology, Diabetes and Metabolism, Sheba Medical Center, Tel Hashomer, Israel

ABSTRACT

Autonomous finite element analyses (AFE) based on CT scans predict the biomechanical response of femurs during stance and side-wise fall positions. We combine AFE with patient data via a machine learning (ML) algorithm to predict the risk of hip fracture. An opportunistic retrospective clinical study of CT scans is presented, aimed at developing a ML algorithm with AFE for hip fracture risk assessment in type 2 diabetic mellitus (T2DM) and non-T2DM patients.

Abdominal/pelvis CT scans of patients who experienced a hip fracture within 2 years after an index CT scan were retrieved from a tertiary medical center database. A control group of patients without a known hip fracture for at least 5 years after an index CT scan was retrieved. Scans belonging to patients with/without T2DM were identified from coded diagnoses. All femurs underwent an AFE under three physiological loads. AFE results, patient's age, weight, and height were input to the ML algorithm (support vector machine [SVM]), trained by 80% of the known fracture outcomes, with cross-validation, and verified by the other 20%.

In total, 45% of available abdominal/pelvic CT scans were appropriate for AFE (at least 1/4 of the proximal femur was visible in the scan). The AFE success rate in automatically analyzing CT scans was 91%: 836 femurs we successfully analyzed, and the results were processed by the SVM algorithm. A total of 282 T2DM femurs (118 intact and 164 fractured) and 554 non-T2DM (314 intact and 240 fractured) were identified. Among T2DM patients, the outcome was: Sensitivity 92%, Specificity 88% (cross-validation area under the curve [AUC] 0.92) and for the non-T2DM patients: Sensitivity 83%, Specificity 84% (cross-validation AUC 0.84).

Combining AFE data with a ML algorithm provides an unprecedented prediction accuracy for the risk of hip fracture in T2DM and non-T2DM populations. The fully autonomous algorithm can be applied as an opportunistic process for hip fracture risk assessment.

© 2023 The Authors. *Journal of Bone and Mineral Research* published by Wiley Periodicals LLC on behalf of American Society for Bone and Mineral Research (ASBMR).

KEY WORDS: DIABETES MELLITUS; HIP FRACTURE; FINITE ELEMENT ANALYSIS; FRACTURE RISK ASSESSMENT; SVM/MACHINE LEARNING

Introduction

Hip fractures are among the most common reasons for orthopedic hospitalization in the elderly worldwide,

leading to major health and financial burden.⁽¹⁾ The underlying cause of such fractures is most often osteoporosis. Pharmacological treatments are usually prescribed to prevent hip fractures by patients identified to be at high risk. Although the strength of the

This is an open access article under the terms of the [Creative Commons Attribution-NonCommercial](#) License, which permits use, distribution and reproduction in any medium, provided the original work is properly cited and is not used for commercial purposes.

Received in original form November 9, 2022; revised form March 7, 2023; accepted March 21, 2023.

Address correspondence to: Zohar Yosibash, DSc, School of Mechanical Engineering, The Iby and Aladar Fleischman Faculty of Engineering, Tel Aviv University, Ramat Aviv, Tel Aviv, Israel. E-mail: yosibash@tauex.tau.ac.il

ZY and NT contributed equally to this work.

Journal of Bone and Mineral Research, Vol. 00, No. 00, Month 2023, pp 1–11.

DOI: 10.1002/jbmr.4805

© 2023 The Authors. *Journal of Bone and Mineral Research* published by Wiley Periodicals LLC on behalf of American Society for Bone and Mineral Research (ASBMR).

hip is a function of its mechanical material properties, geometry, and loading, most risk assessments use bone mineral density as a surrogate for bone strength. Hip fracture risk is usually determined by dual-energy X-ray absorptiometry (DXA) measurement of femoral neck areal bone mineral density (aBMD) or by the Fracture Risk Assessment Tool (FRAX), which is based on 11 clinical factors along with femoral neck aBMD. Neither of these tools is accurate, especially for type 2 diabetic mellitus patients (T2DM). These patients are at a twofold greater risk of hip fractures and display a “diabetic paradox”: increased risk of femoral fractures despite having higher bone mineral density.⁽²⁻⁷⁾ The trabecular bone score (TBS) is an indirect index of trabecular architecture applied to infer information from spine DXA image but is assessed only for vertebral fracture risk^(7,8) and cannot be applied to the proximal femur.

Finite element analyses of proximal femurs based on computed tomography scans (CTFEA) have been developed for predicting femur stiffness and hip fracture risk. CTFEA has been shown to outperform DXA.⁽⁹⁻¹⁴⁾ The practical use of the technology has been hampered by the high patient radiation exposure, the expense of CT scans, and the lack of fully automated FEA calculations. A large number of abdominal and pelvic CT scans are available in hospitals or health maintenance organization (HMO) picture archiving and communication systems (PACS). These scans also usually include the hip and the lesser tuberosity of the femur. They may, therefore, be potentially used opportunistically for hip FEA without exposing patients to additional radiation hazards.⁽¹⁵⁾

We have developed (Simfina is a product of PerSimiO Ltd, Beer-Sheva, Israel)⁽¹⁶⁾ as an autonomous CTFEA software application for the FEA of femurs. This tool has been shown to provide accurate predictions of pathological hip fractures in patients with metastatic tumors in two retrospective clinical studies.^(17,18)

Recently Simfina's performance in predicting hip risk of fracture was also examined in a feasibility retrospective clinical study on a cohort of 51 T2DM patients.⁽¹⁹⁾ This system includes several novel features:

1. It is fully autonomous, with no manual subjective intervention.
2. The two femurs (left and right) are automatically segmented from the CT scan by means of a deep learning (DL) algorithm and thereafter automatically represented by a mesh of high-order finite elements.
3. Physiological loading conditions are simulated that represent the two common sidewise falls resulting in neck and intertrochanteric fractures.
4. A machine learning (ML) algorithm is used in the post-autonomous finite element (AFE) stage, which accounts for patients' weight, height, sex, and the biomechanical results at different regions along the proximal femur.

We undertook a retrospective clinical study to assess the performance of the Simfina system in predicting the risk of hip fracture in type 2 diabetic and non-diabetic patients, based on opportunistic abdominal and pelvic CT scans obtained from the PACS of a major medical center.

Methods

Study design

The Sheba Medical Center (MC) database was searched for patients with CT scans of the lower abdomen/pelvis between

2008 and 2020 who experienced a hip fracture (study group) during the subsequent 2 years. Both non-contrast and contrast-enhanced CT scans were considered. The control group included age- and weight-matched patients with CT scans who did not sustain a hip fracture in the subsequent 5 years (a conservative requirement to make sure that patients indeed are risk-free for a much longer period than compared with the study group) according to the electronic medical record. The CT scans were collected from the hospital's clinic registry at Sheba MC. Approval was granted by the Sheba MC institutional review board (7969-20-SMC). Overall, 974 CT scans were collected for the study.

The primary outcome was a binary score of the risk of hip fracture within 2 years after the CT scan or a non-fracture risk within 5 years after the CT scan. The results obtained from the combined AFE&ML system were used as a risk factor for sustaining a hip fracture.

Patient population

Inclusion criteria included CT scans with a soft tissue filter and 120 Peak kiloVoltage (KVP). Exclusion criteria included: (i) pathologic fractures, subtrochanteric or atypical fractures, high-energy fractures, metallic implants, and tumors in the proximal femur; (ii) type 1 diabetes mellitus. Of the 974 CT scans, 507 were excluded because of misfit to the clinical trial protocol. The data set workflow is presented in Fig. 5.

For each patient, clinical data, including the weight, age, height, and whether he/she was diagnosed with T2DM, were retrieved from the electronic records.

AFEs

The fully autonomous CTFEA system Simfina was used to perform the strength analysis of all femurs according to the algorithm previously published^(16,17,19,20) and schematically illustrated in Fig. 1. Briefly, the geometry of the femurs is automatically segmented from the CT scans by a deep-learning U-Net network to produce a 3D voxel representation of the femur. Inhomogeneous isotropic material properties are assigned to the centroid of each voxel within the femur based on the Hounsfield unit (HU) in the CT scan. The voxels representing the segmented femur are automatically transformed in a mesh of high-order tetrahedral elements. High order elements have shape functions with a polynomial degree increased hierarchically from 1 to 8 (each tetrahedral element has 512 shape functions at $p=8$), allow for curved edges, and allow the intrinsic estimation of the error in energy norm since 8 hierarchical FE solutions with increasing number of degrees of freedom are obtained. A special numerical integration scheme is used that facilitates exact integration of monomials up to 14th order. Three loading configurations were applied as presented in Fig. 2, and average maximum principal strains were extracted automatically over a circular region of a diameter of 5 mm on the surface of the femur in each region of interest.

The three different boundary conditions applied to each femur

A proximal femoral fracture resulting from a fall on the side is categorized as either a neck or a pertrochanteric fracture, with an almost equal probability to occur.^(21,22) Two different load directions induce two different fracture scenarios. These directions were determined by a former clinical study on 32 patients who

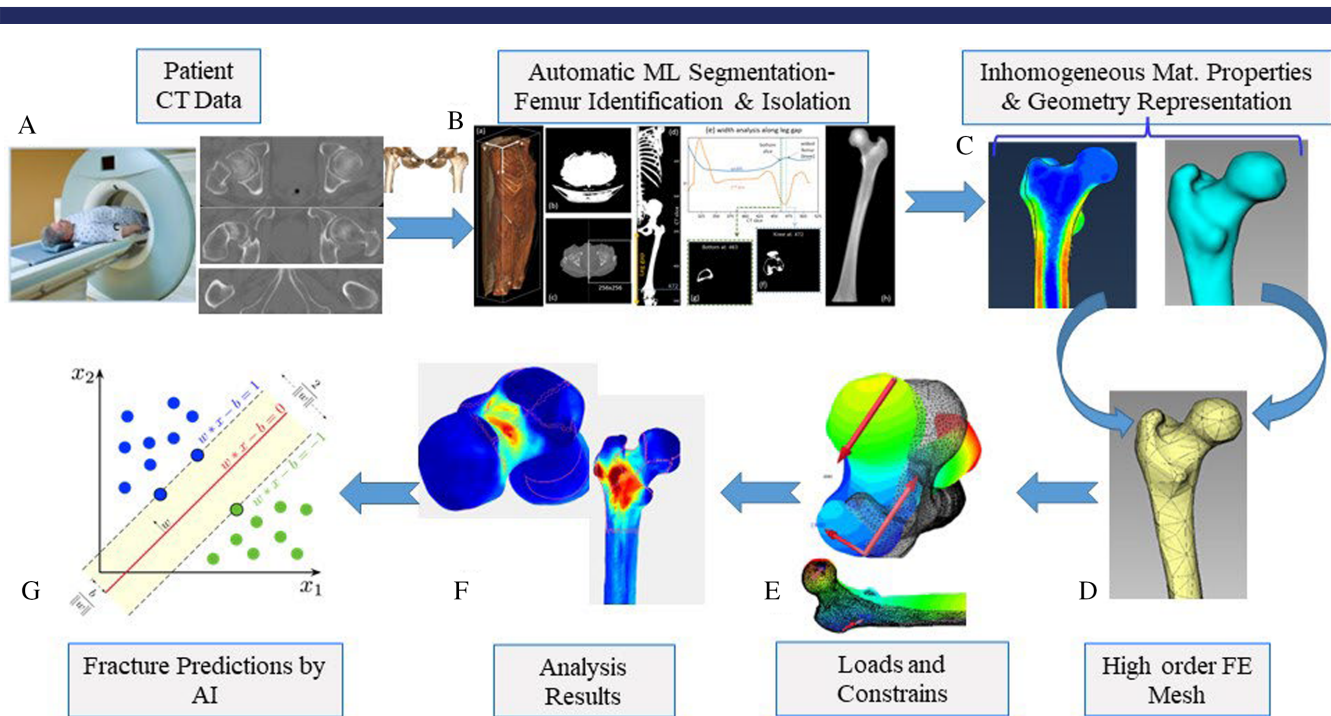


Fig. 1. Schematic description of the Simfini system. (A) Retrieval of CT scans from picture archiving and communication system (PACS). (B) Segmentation of the two femurs by U-Net and identification of anatomical points. (C) Generation of the inhomogeneous material data and 3D geometry of both femurs. (D) Generating a high-order finite element (FE) mesh. (E) Application of three different boundary conditions and solution of the FE system. (F) Extraction of averaged maximum strains at different locations along the femur. (G) Fracture predictions by support vector machine (SVM) algorithm. DL = deep learning; ML = machine learning.

experienced a hip fracture and were CT scanned immediately after the fracture. Fourteen patients were diagnosed as having a neck fracture ($f = 8, m = 6$) and 18 were diagnosed as having a pertrochanteric fracture ($f = 12, m = 6$).⁽²³⁾ For the neck fracture group, loading configuration *FallN* (Fig. 2) always stresses the superior and inferior neck with the lowest fracture load and was selected as a good predictor for a femoral neck fracture. For the pertrochanteric fracture, loading configuration *FallP* (Fig. 2) stresses in most of the cases the trochanter but also the anterior and posterior base of the neck. The loading condition was selected as the preferred predictor for trochanteric fracture (see also in vitro experiments: "...FE models predicted that the fractures initiate under compression on the lateral side of the femoral neck"⁽²⁴⁾). Illustrative examples of the two loading conditions and the maximum compressive strained locations are presented in Fig. 2. *FallN* predicts a neck fracture at the superior neck in compression. *FallP* also predicts a pertrochanteric fracture in compression. Therefore, it is conceivable to consider both. The application of multiple loading conditions to best represent a sidewise fall condition has been confirmed by in vitro experiments: "FE-strength from multiple loading conditions better-classified fracture cases from controls... Only FE-strength from multiple loading conditions remained significant in age- and aBMD-adjusted models"⁽²⁵⁾.

Stance loading (along the vector connecting the head and intercondylar notch) also induces high strains in the superior and inferior neck regardless of the fracture's actual location. AFE results under this loading condition are also considered when determining the risk of fracture. The magnitude of all

loads is normalized by the patient's body weight. In the AFE, the total magnitude of all applied loads is 2.5 times the patient's weight.

Because the γ and δ angles are determined by anatomical points, the algorithm performs best if at least 20 mm below the lesser trochanter is visible in the CT scan. A borderline case is when only the lesser trochanter is visible. CT scans that do not include the entire lesser trochanter are disqualified from being biomechanically analyzed.

Average maximum principal tensile strains (denoted by E1) and average minimum principal compression strains (denoted by E3) are automatically computed in each of the areas of interest, for each loading condition: neck superior and inferior, trochanter posterior and anterior, head superior and inferior, and lesser trochanter inferior (Fig. 3). Head movement and bone stiffness (force magnitude divided by head movement) as well as moment applied and maximum and minimum Young's modulus in the femur are also computed.

Combining biomechanical data with patient data and application of machine learning techniques

Statistical learning models, and particularly ML, have been recently used to automatically post-process many data combinations.⁽²⁶⁾ Here, we present a ML model that combines patient data with computational biomechanics results to predict the risk of hip fractures. The ML model was trained separately for the T2DM group and the non-T2DM group.

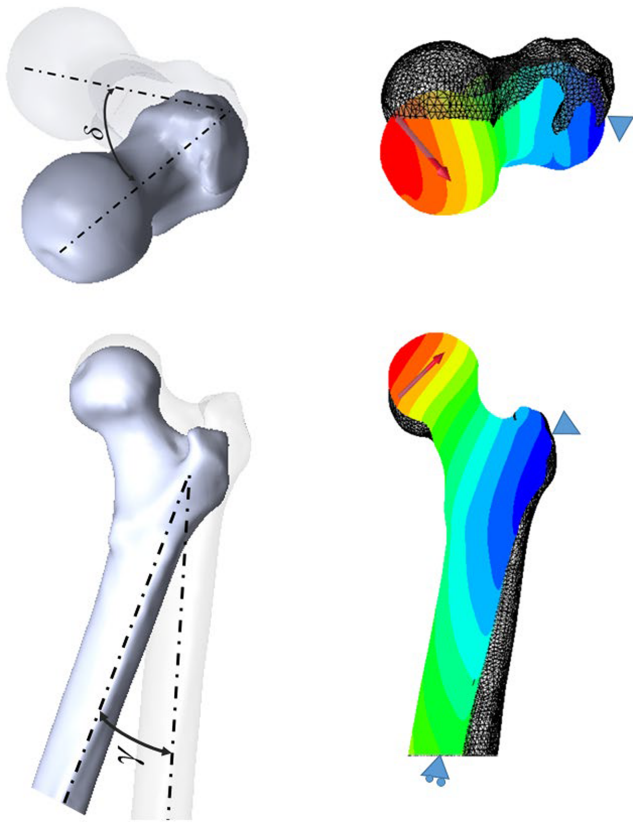


Fig. 2. Definition of boundary conditions for sideways fall configuration. FallIN is determined by $\gamma = 10^\circ$ and $\delta = 15^\circ$ and FallP by $\gamma = 30^\circ$ and $\delta = 45^\circ$. Figures with colors representing displacements due to boundary conditions are taken from Rotman and colleagues.⁽¹⁹⁾

The available samples were shuffled and split 0.8 for training and 0.2 for testing. Because of the small train set, we used cross-validation over the train set only. Cross-validation is a technique that allows one to estimate the performance of machine learning models on unseen data. We applied the k -fold cross-

validation method, where the data were divided into $k = 6$ subsets. The model was then trained on 5 of these subsets and evaluated on the remaining one. This process was repeated 6 times, with each subset being used as the validation set once (Fig. 5). We calculated the mean and standard deviation of all statistical metrics (F1, precision, etc.) over the left-out subsets to ensure the chosen threshold is a good fit for our model to verify its generalization ability. In that manner, we were able to obtain an estimate of the model's performance that is not affected by the specific data used for training and validating. Then, we applied the model, with the chosen threshold, over the independent test set (the remaining 20% of the data).

The available patient data set is unbalanced; thus, we had to prevent the ML model from becoming biased toward the predominant class. We used random oversampling to balance the unbalanced training data set, ie, balancing the data by replicating the minority class samples (a method that does not cause any loss of information⁽²⁷⁾). Oversampling was not used either for the folded-out set in each training/validation split or for the independent testing set that was separated at the preprocessing procedure. Each data set was normalized by removing the mean and scaling each feature to unit variance. The training samples are given to the model for creating the inference mapping function from the domain of features to the label domain—trying to maximize the number of samples classified correctly but keeping the problem generalized and not overfit. The testing/validation samples are the new cases not used for training the ML process. Based on these, the predicted specificity and sensitivity are computed (thanks to a comparison of the real known labels with the model-predicted ones).

We considered two ML algorithms: random forest (RF) and support vector machine (SVM).⁽²⁸⁾ Both algorithms are well suited for a mixture of numerical and categorical features. The SVM training algorithm constructs a model that maps training examples to points in space to maximize the width of the gap between the two categories. New examples are then mapped into that same space and predicted to belong to a category based on which side of the gap they fall. A detailed discussion on SVM, including the mathematical foundations and the various factors that influence its performance, is provided in Cristianini and Shawe-Taylor.⁽²⁹⁾ The dominant factor we used is the ν parameter to control the number of support vectors.⁽³⁰⁾

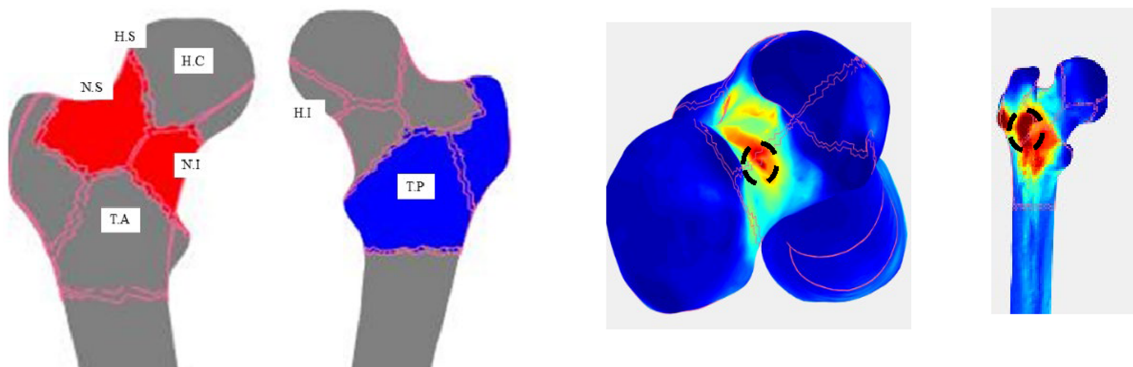


Fig. 3. The various locations (head superior, head inferior neck superior, neck inferior, trochanter posterior, trochanter anterior, head center) in the proximal femur at which strains are computed by the autonomous finite element (AFE) analysis (left two figures) and maximum compressive principal strains at the neck and intertrochanteric regions due to two different sideways fall loadings (right two figures).

RF is an ensemble learning method for classification that operates by constructing a multitude of decision trees at training time. For classification tasks, the output of the RF is the class selected by most trees. Random decision forests correct for decision trees' tendency to overfit to their training set.

RF and SVM fracture/non-fracture predictions for the two groups were compared based on the receiver-operating characteristic curve (ROC) and the area under the curve (AUC). The operating point threshold for the inference model was chosen at the point with the highest F1 score for the cross-validation set. Both RF and SVM results are very similar with slightly better performance for the SVM. Therefore, SVM was the chosen method. The sensitivity, specificity, and AUC of the SVM for the T2DM group and the non-T2DM group (computed based on 20% of the CT scans) are presented in Results. A total of 41 features were used in the SVM algorithm as detailed in Table 1.

Statistical analysis and verification of results

The predictive performance of the risk of fracture criteria was evaluated for its specificity, sensitivity, and AUC as follows. "Sensitivity" is defined as the percentage of patients for whom fractures were correctly predicted and occurred within 2 years of the CT scan. "Specificity" is defined as the percentage of patients correctly identified as fracture-free for 5 years after the scan. To determine the uncertainty of the estimates of sensitivity and specificity, 95% confidence intervals (CIs) are calculated for the test set according to Ying and colleagues.⁽³¹⁾

The ROCs were generated and the AUCs were computed and reported.

To further verify the performance once the algorithm was established, the SVM was applied to the 17 additional CT scans for which only one femur was successfully analyzed (due to presence of an implant, preexisting fracture, etc.). Within this cohort, 13 patients were non-T2DM, 7 experienced a hip fracture, and 6 with intact femurs. Four patients were T2DM, 2 experienced a hip fracture, and 2 with intact femurs.

Results

A total of 974 clinical CT scans were retrieved, generated by several different scanners (manufactured by GE [Madison, WI, USA] and Philips [Andover, MA, USA]). Pixel spacing for the scans was between 0.57 and 0.98 mm. Although slice thickness was between 0.63 and 3 mm, most scans had a 2 mm slice thickness. No duplicate CT scans for any patients were identified in the cohort. Patients of the study group were selected by one of the researchers (EK), who was blind to the content of the scans: A list of CT accession numbers was generated from the Sheba Medical Center radiology department information system. Then, the corresponding CTs were retrieved from the Sheba Medical Center radiology department PACS in Digital Imaging and Communications in Medicine (DICOM) format after anonymization of the DICOMs meta-data fields.

A total of 507 CTs were excluded from the study for not complying with the protocol (the majority because the femur was "short" a "short" CT is defined as a CT which does not

Table 1. List of 41 Features Used in the Support Vector Machine Algorithm: 37 Generated by the Autonomous Finite Element Analysis and last 4 Related to Patient Data

'Stance neck superior E1'	'Stance trochanter E1'	'Stance neck inferior sub capital E3'	'Stance trochanter E3'	Stance head center Utot	Stance bone K	'FallN neck inferior E1'	'FallN trochanter posterior E1'	'FallN lesser trochanter anterior E1'	'FallN head superior E1'	'FallN head inferior E1'
'FallN Neck Superior E3'	'FallN Neck Inferior E3'	'FallN Trochanter Posterior E3'	'FallN Lesser Trochanter Anterior E3'	'FallN Head Superior E3'	'FallN Head Inferior E3'	FallN Head Center Utot	FallN Bone K	'FallP Neck Superior E1'	'FallP Neck Inferior E1'	'FallP Trochanter Posterior E1'
'FallP Lesser Trochanter Anterior E1'	'FallP Head Superior E1'	'FallP Head Inferior E1'	'FallP Neck Superior E3'	'FallP Neck Inferior E3'	'FallP Trochanter Posterior E3'	'FallP Lesser Trochanter Anterior E3'	'FallP Head Superior E3'	'FallP Head Inferior E3'	FallP Bone K	FallP Bone K
'Femoral length mm'	'E max'	'E min'	'Mtot Stance at 80 mm below top'	Age	Height	Weight	Sex			



Fig. 4. Illustrative examples of short (left), borderline (middle), and standard (right) femurs in CT scans.

Table 2. Summary of Standard/Borderline Femurs for the Study and Control Groups That Were Successfully Analyzed by Simfina

	Standard	Border	Total
No. of femurs without a fracture within 5 years after CT	204	274	478
No. of fractured femurs	104	254	358
Total	308	528	836

contain at least the lesser trochanter of one of the two femurs in the scan.). CT scans in which the lesser trochanter is visible but included less than 20 mm below the trochanter were denoted “borderline.” Typical examples of short, borderline, and standard CT scans are shown in Fig. 4. CTs were excluded if:

1. The CT scan did not include the entire lesser trochanter.
2. A metallic implant was present that resulted in artifacts in the proximal femur.
3. Tumors were clearly visible in the proximal femur.
4. A fracture was reported, but it was either caused by a high-energy trauma or occurred in the distal femur.

A total of 467 CTs (standard and borderline) were suitable for Simfina analysis (48% of all CT scans collected). Twenty-two of these could not be retrieved successfully from the PACS, Simfina issued an error message for 12 CTs (failed to segment the femur or to generate a finite element mesh), and for 17 CTs, the analysis was successful for one femur only. Therefore, the success rate of Simfina was $(934-44-24-17)/934 = 91\%$, resulting in data for 836 femurs representing 418 CT scans. Table 2 summarizes the number of standard and borderline femurs in the study and control group. None of the scans had calibration phantoms. Overall, 568 femurs were acquired by GE scanners and 268 femurs by Philips scanners.

A flowchart illustrating the femur selection process for the Simfina analysis is presented in Fig. 5.

Table 3 summarizes the distribution of the 836 femurs of T2DM and non-T2DM patients that were successfully analyzed by Simfina.

Table 4 summarizes the average age, weight, and height of the patients for whom Simfina analyses were successfully performed.

There were no statistically significant differences between the study and the control groups regarding age, weight, and height (Table 4).

For each patient, the strains computed by Simfina under the different loading conditions were extracted and shown as an example for *FallN* and *FallP* in Fig. 6.

The SVM cross-validation performance is summarized in Table 5 and the corresponding ROC curves are presented in Fig. 7. The AUC values for the ROC curves are also reported in Table 5. The SVM test set predictions are summarized in Table 6. The *p* value of all data set configurations was less than 0.01.

It is important to emphasize that no attempt was made to optimize the outcome of the SVM algorithm by including or excluding input features.

Further verification

The 17 patients for whom the AFE failed to analyze both femurs were not included in the SVM analysis but were used for further verification of the accuracy in predicting hip fracture risk.

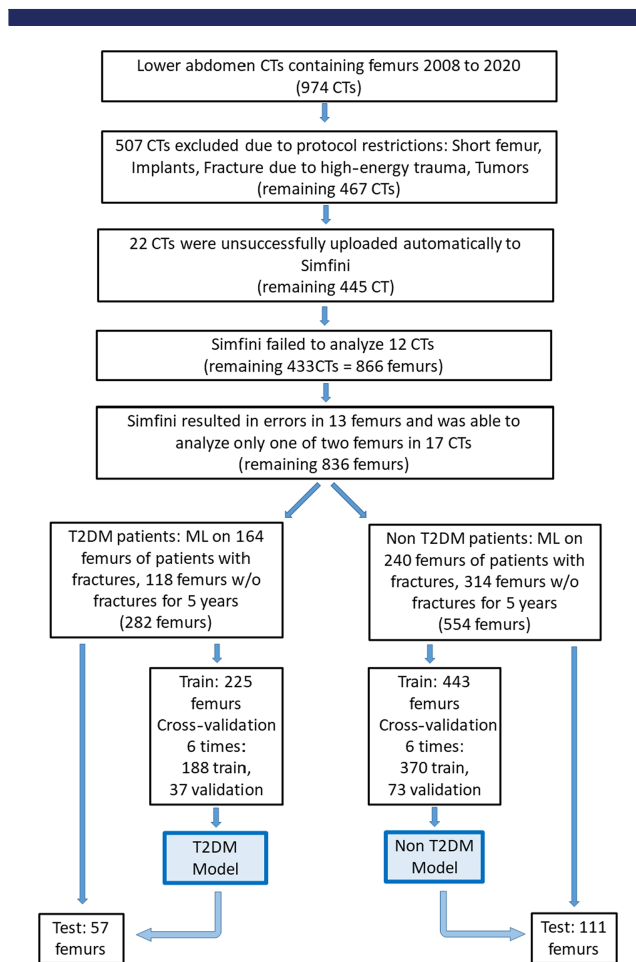


Fig. 5. Case selection process.

Table 3. Summary of the Number of Femurs for T2DM and Non-T2DM Patients Successfully Analyzed by Simfina

	Intact	Fractured	Total
T2DM patients	118	164	282
Non-T2DM patients	314	240	554
Total	432	404	836

Using the AFE results for one femur and the trained SVM algorithm, the following statistics were obtained: for the 4 T2DM patients, the sensitivity was 100% and the specificity was 67%. For the non-T2DM patients (13 patients), the sensitivity was 75% and the specificity was 80%.

DXA data

Only 11 of the 418 patients who were AFE analyzed had available DXA scores in the Sheba MC database: 2 T2DM patients, one who fractured and one who did not, both had a *T*-score of -1.5 at the proximal femur and -1.9 , -2.0 at the lower neck. Among the 9 non-T2DM patients, 3 fractured with a *T*-score of -1.5 , -1.9 , -2.2 at the proximal femur and -1.6 , -2.2 at the neck. Six non-T2DM patients who did not fracture had a *T*-score between

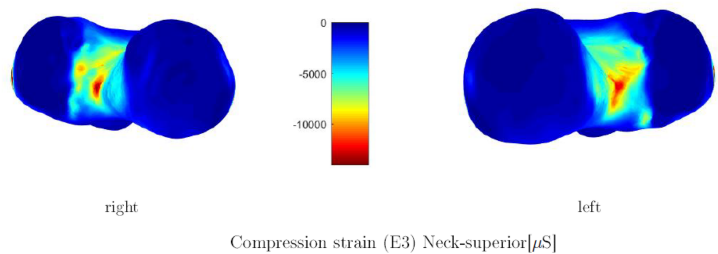
Table 4. Summary of Age, Weight, and Height (With Standard Deviation) and Sex for Patients Successfully Analyzed by Simfini (418 CT Scans; 836 Femurs)

	No. of CTs	Male/Female	Average age (years)	Average weight (kg)	Average height (cm)
Fx T2DM	82	35 M/47 F	75.8 ± 8.4	71.5 ± 15.8	164 ± 8.6
Intact T2DM	59	19 M/40 F	77.5 ± 9.4	69.3 ± 16.3	163 ± 9.7
Fx non-T2DM	157	46 M/111 F	75.8 ± 9.4	66.0 ± 17.4	163 ± 8.8
Intact non-T2DM	120	36 M/82 F	75.9 ± 9.3	67.8 ± 13.3	162 ± 8.6



4.2 Results table- side fall N configurations

Region	Value			
	E1		E3	
	Right	Left	Right	Left
Neck Superior	4836	4431	-12544	-12010
Neck Inferior	3898	3596	-6844	-6197
Trochanter Posterior	4928	5287	-6659	-5713
Lesser Trochanter Anterior	3197	2906	-1979	-2050
Head Superior	2281	1893	-4400	-4681
Head Inferior	3524	2329	-2906	-2963
Proximal Shaft	2880	2521	-3926	-3739



4.4 Results table- side fall P configurations

Region	Value			
	E1		E3	
	Right	Left	Right	Left
Neck Superior	8724	7512	-11602	-10292
Neck Inferior	6209	5619	-10070	-8001
Trochanter Posterior	9328	12594	-10401	-9660
Lesser Trochanter Anterior	6188	4946	-3499	-3570
Head Superior	2759	3013	-4622	-4968
Head Inferior	3990	4851	-2777	-5135
Proximal Shaft	5895	5489	-7923	-7992

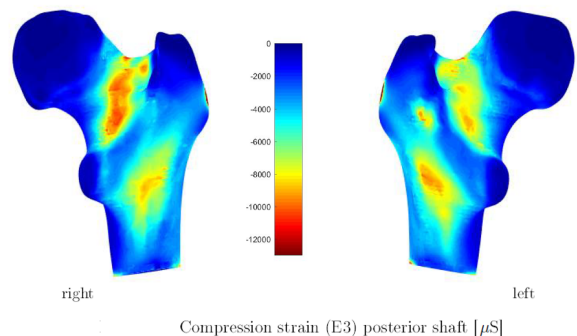


Fig. 6. Simfini computed strains (tensile E1 and compressive E3) under FallN and FallP loadings (2.5 body weights) for a typical patient.

0.5 and -1.4 at the proximal femur and -0.4 to -2.2 at the neck. None of the 4 who fractured had a T -score below -2.5 , ie, diagnosed as osteoporotic. The DXA data are too limited for statistical analysis; however, it shows that none of those who fractured had a densitometric diagnosis of osteoporosis (the average age was 75 years, similar to the AFE cohort).

Discussion

Simfini is a fully autonomous finite element system that can be easily used for opportunistic biomechanical analysis of abdomen or pelvis CT scans of the femur. The biomechanical analysis is fused to an ML (SVM) algorithm and provides highly accurate hip fracture risk prediction in elderly T2DM and non-T2DM populations. A total of 48% of the abdominal and pelvic CT scans evaluated were appropriate for the AFE (very similar to the percentage reported in Michalski and colleagues⁽¹⁴⁾), of which

91% were successfully analyzed by the AFE (ie, 43% of the available lower abdomen and pelvic CT scans were successfully analyzed). An excellent prediction of hip fractures within the next 2 years for both T2DM patients (a group that possesses a special challenge) as well as non-T2DM ones was shown.

The further verification on 17 patients for whom the AFE was able to analyze only one femur showed that the outcome corresponds well with the statistical data presented.

The CT utilization rate in our study is on par with other published studies using opportunistic screening tools: Dagan and colleagues reported an 83.6% utilization rate⁽³²⁾ and Adams and colleagues reported an 86% utilization rate,⁽¹³⁾ both in very large and diverse populations.

During the past 5 years, several studies have shown the feasibility of using opportunistic CT scans to predict osteoporotic fractures,⁽³³⁾ specifically hip fractures.^(9,34) The only autonomous algorithm (based entirely on ML)⁽³²⁾ was trained and verified on more than 48,000 CT scans to assess the 5-year risk of

Table 5. Support Vector Machine Cross-Validation Predictions Mean Values and Standard Deviation (in Parentheses) of the Sensitivity, Specificity, Precision, and Area Under the Curve (AUC)

Mean (SD)	F1 score	Sensitivity (SD)	Specificity (SD)	Precision	AUC for the cross-validation set
T2DM cross-validation	0.81 (0.03)	0.77 (0.09)	0.82 (0.04)	0.89 (0.06)	0.92
Non-T2DM cross-validation	0.78 (0.04)	0.81 (0.08)	0.80 (0.05)	0.79 (0.05)	0.84
Combined T2DM and Non-T2DM Cross-validation	0.78 (0.02)	0.8 (0.03)	0.78 (0.06)	0.83 (0.04)	0.88

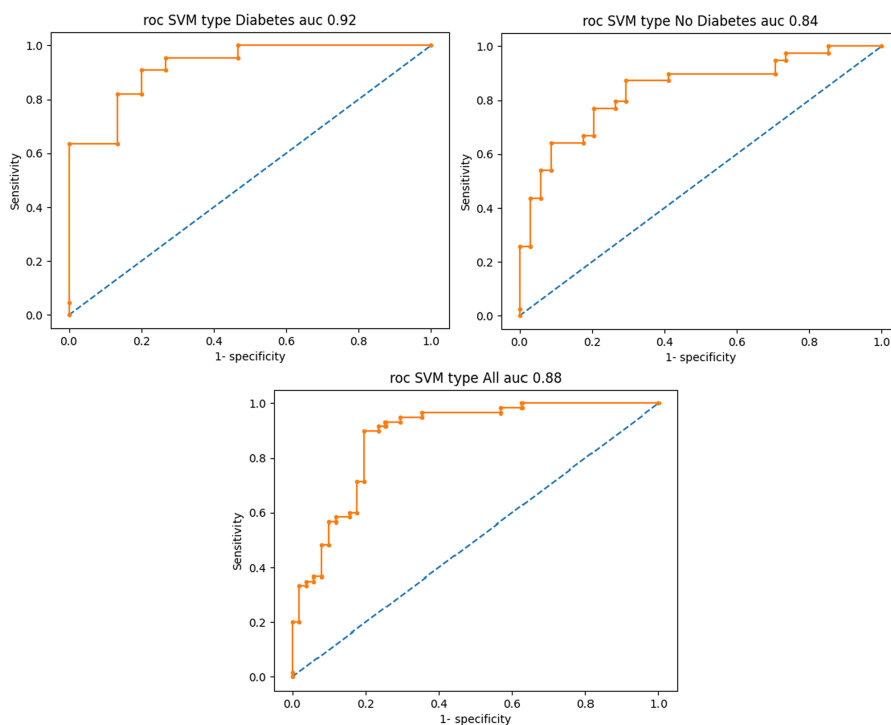


Fig. 7. Receiver operating characteristic (ROC) curves for the T2DM population (upper left), the non-T2DM population (upper right), and the combined T2DM and non-T2DM population (lower middle) for the cross-validation set, showing an area under the curve (AUC) of 0.92, 0.84, and 0.88, respectively.

Table 6. Support Vector Machine Test Set Predictions in Terms of Sensitivity, Specificity (With 95% Confidence Interval [CI]), and Precision

	F1 score	Sensitivity (95% CI)	Specificity (95% CI)	Precision
T2DM – Test set	0.84	92% (85–99%)	88% (80–97%)	0.85
Non-T2DM – Test set	0.81	83% (76–90%)	84% (77–91%)	0.86
Combined T2DM and non-T2DM cross-validation	0.82	86% (73–89%)	79% (75–82%)	0.85

osteoporotic fractures. The ML predictions for a hip fracture were shown to be the same as the FRAX performance without BMD input. The ML algorithm relies mostly on BMD assessment from CT scans. A sensitivity of 92.6%, specificity of 36.9%, and AUC of 0.76 were achieved, which were almost identical to FRAX performance.⁽³²⁾

FEA determination of femoral strength has been shown to better predict hip fracture than hip BMD.^(35,36) Several previous studies have shown the use of femoral strength measurement derived from existing CT scans to predict hip fracture risk.^(11,13,14) In Adams and colleagues,⁽¹³⁾ 1959 patients aged 65 years or older who sustained a hip fracture and who had a prior pelvic or abdominal CT scan and a DXA were compared with a sex-matched group.

The study population included 30% diabetic patients, but there was no subanalysis to determine the validity of this method specifically in those patients. In Michalski and colleagues,⁽¹⁴⁾ 490 lower-abdomen CT scans of 1158 were suitable for FEA (43.2%), of which 123 suffered a fracture within 5 years of the CT scan date. Fracture prediction by combining both BMD and FE-estimated bone strength was not statistically different from using either BMD or FE-estimated bone strength alone. Predicting fractures in women determined the greatest AUC of 0.710 by using both BMD and FEA (sensitivity 48% and specificity 84%). The study reported in Fleps and colleagues⁽¹¹⁾ used very uniform CT scans, all resulting from a single CT scanner with a slice thickness of 1 mm and all having calibration phantoms. This database was unusual because

Table 7. Summary of the Performance of Recent Methods for Identifying Risk of Hip Fractures: Number of CTs Considered, Sensitivity, Specificity, and Area Under the Curve (AUC)

Method (ref)	No. of CTs	Sensitivity	Specificity	AUC
Current CTFEA + ML T2DM (cross-validation set)	141	92% (77%)	88% (82%)	(0.92)
Current CTFEA + ML non-T2DM (cross-validation set)	277	83% (81%)	84% (80%)	(0.84)
Current CTFEA + ML combined (cross-validation set)	418	86% (80%)	79% (78%)	(0.88)
CTFEA + aBMD ⁽¹⁴⁾	490	48%	84%	0.71
CTFEA ⁽¹¹⁾	601			0.71–0.80
Women CTFEA ⁽¹³⁾	~1900	66%	66%	0.70–0.73
Men CTFEA ⁽¹³⁾	~860	56%	76%	0.75
ML ⁽³²⁾	~48,000	92.6%	36.9%	0.76
CTFEA T2DM ⁽¹⁹⁾	51	89%	76%	0.9

typical clinical scans are from a variety of CT scanners, have lower resolution, and none use calibration phantoms.

CTFEA accurately predicts one of the most important components required to determine the risk of femoral fracture—the bone strength under a load that is believed to represent a side-wise fall. One of the reasons CTFEA is not commonly used in clinical practice is the manual labor and expertise required to set up the analysis and interpret the output, which may be a lengthy and subjective process. Also, the patient’s weight was not taken into consideration in former CTFEAs, which in the authors’ opinion is an important component.

To address the perceived need for improved fracture risk assessment, we developed the fully AFE system⁽¹⁶⁾ that automatically retrieves CT scans from a hospital’s PACS, segments the femurs by a DL algorithm, automatically performs FE analyses with physiological loads, and applies a SVM post-processing algorithm. We found the most influential factor over the post processing performance is the ν parameter that controls the number of support vectors. The fully autonomous system showed unprecedented identification of hip fracture risk within 2 years after the CT scan. In Table 7, we summarize the current system’s performance compared with the performance reported in former publications.

In conclusion, this clinical study shows a high accuracy achieved when predicting the risk of fracture resulting from a sidewise fall by combining AFE and machine learning in both T2DM and non-T2DM populations. Because there is a significant clinical need to develop a reliable risk assessment tool for the T2DM population, implementing such a tool as an opportunistic measure on a large scale could contribute significantly to the prevention of osteoporosis-related complications in diabetic patients, specifically hip fractures.

The proposed AFE may be used in many other clinical applications by assessing bones’ strength in longitudinal studies to monitor, for example, radiation therapy influence, medication efficacy, over/under stress, etc. Application of the methodology to other bones such as the humerus, vertebra, and tibia is another promising outcome of the presented methodology.

This study has several limitations: (i) Results were not compared with current commonly used methods to measure bone strength or assess fracture risk, namely a DXA or a FRAX score, as the hospital registry in Israel has very limited data on these for most patients; (ii) CTs that do not include the entire lesser trochanter are excluded from the AFE (about 50% of the overall

lower-abdomen CT); (iii) data on the first diagnosis of T2DM for these patients are missing.

The encouraging results pave the path to further clinical and scientific enhancements. A follow-on research study is planned that will include AFEs of CT scans in which only a part of the lesser trochanter is visible. Although this approach is expected to considerably increase the number of usable femur scans in the study, it will likely see a decrease in sensitivity and specificity of the fracture risk assessment. Optimal input features to the SVM algorithm will also be investigated, and a prospective study is planned to use opportunistic CT scans with corresponding DXA scores to allow direct comparison with the AFE performance.

Acknowledgments

The authors gratefully acknowledge the partial funding by the Israel Innovation Authority for the clinical trial.

Author Contributions

Zohar Yosibash: Conceptualization; methodology; supervision; data curation; writing – original draft; investigation; funding acquisition. **Nir Trabelsi:** Methodology; validation; writing – review and editing; investigation. **Itay Buchnik:** Methodology; formal analysis. **Kent W Myers:** Writing – review and editing; software. **Moshe Salai:** Writing – review and editing; conceptualization. **Iris Eshed:** Writing – review and editing; supervision. **Yiftach Barash:** Data curation. **Eyal Klang:** Data curation. **Liana Tripto-Shkolnik:** Conceptualization; methodology; supervision; writing – review and editing.

Disclosures

ZY, NT, and KWM are founders of and have equity in PerSimiO.

Data Availability Statement

The data that support the findings of this study are available on request from the corresponding author. The data are not publicly available due to privacy or ethical restrictions.

References

- Hernlund E, Svedbom A, Ivergård M, et al. Osteoporosis in the European Union: medical management, epidemiology and economic burden. A report prepared in collaboration with the International Osteoporosis Foundation (IOF) and the European Federation of Pharmaceutical Industry Associations (EFPIA). *Arch Osteoporos*. 2013;8:136.
- Fan Y, Wei F, Lang Y, Liu Y. Diabetes mellitus and risk of hip fractures: a meta-analysis. *Osteoporos Int*. 2016;27(1):219–228.
- Botella Martinez S, Cenarruzabeitia NV, San Martin JE, Canelas AC. The diabetic paradox: bone mineral density and fracture in type 2 diabetes. *Endocrinol Nutr*. 2016;63(9):495–501.
- Schwartz AV, Vittinghoff E, Bauer DC, et al. Association of BMD and FRAX score with risk of fracture in older adults with type 2 diabetes. *JAMA*. 2011;305(21):2184–2192.
- Giangregorio LM, Leslie WD, Lix LM, et al. FRAX underestimates fracture risk in patients with diabetes. *J Bone Miner Res*. 2012;27(2):301–308.
- Ferrari SL, Abrahamsen B, Napoli N, et al. Diagnosis and management of bone fragility in diabetes: an emerging challenge. *Osteoporos Int*. 2018;29(12):2585–2596.
- Schacter GI, Leslie WD. DXA-based measurements in diabetes: can they predict fracture risk? *Calcif Tissue Int*. 2017;100(2):150–164.
- Rubio JB, del Río Barquero L, Olmos JM, Montoya-García M-J, Muñoz-Torres M. Review of the scientific evidence regarding clinical use of the trabecular bone score (TBS). SEIOMM official position. *Rev Osteoporos Metab Miner*. 2018;10(4):149–159.
- Johannesdottir F, Allaire B, Bouxsein ML. Fracture prediction by computed tomography and finite element analysis: current and future perspectives. *Curr Osteoporos Rep*. 2018;16(4):411–422.
- Johannesdottir F, Allaire B, Bouxsein ML. Correction to: fracture prediction by computed tomography and finite element analysis: current and future perspectives. *Curr Osteoporos Rep*. 2022;20(5):364.
- Fleps I, Pálsson H, Baker A, et al. Finite element derived femoral strength is a better predictor of hip fracture risk than aBMD in the AGES Reykjavik study cohort. *Bone*. 2022;154:116219.
- van den Munckhof S, Zadpoor AA. How accurately can we predict the fracture load of the proximal femur using finite element models? *Clin Biomech*. 2014;29(4):373–380.
- Adams AL, Fischer H, Kopperdahl DL, et al. Osteoporosis and hip fracture risk from routine computed tomography scans: the fracture, osteoporosis, and CT utilization study (FOCUS). *J Bone Miner Res*. 2018;33(7):1291–1301.
- Michalski AS, Besler BA, Burt LA, Boyd SK. Opportunistic CT screening predicts individuals at risk of major osteoporotic fracture. *Osteoporos Int*. 2021;32(8):1639–1649.
- Aggarwal V, Maslen C, Abel RL, et al. Opportunistic diagnosis of osteoporosis, fragile bone strength and vertebral fractures from routine CT scans; a review of approved technology systems and pathways to implementation. *Ther Adv Musculoskelet Dis*. 2021;13:1759720X211024029.
- Yosibash Z, Myers K, Trabelsi N, Sternheim A. Autonomous FEs (AFE)—a stride toward personalized medicine. *Comput Math Appl*. 2020;80(11):2417–2432.
- Sternheim A, Giladi O, Gortzak Y, et al. Pathological fracture risk assessment in patients with femoral metastases using CT-based finite element methods. A retrospective clinical study. *Bone*. 2018;110:215–220.
- Sternheim A, Traub F, Trabelsi N, et al. When and where do patients with bone metastases actually break their femurs? *Bone Joint J*. 2020;102-B(5):638–645.
- Rotman D, Ariel G, Lievano JR, et al. Assessing hip fracture risk in type-2 diabetic patients using CT-based autonomous finite element methods: a feasibility study. *Bone Joint J*. 2021;103-B(9):1497–1504.
- Yosibash Z, Trabelsi N, Milgrom C. Reliable simulations of the human proximal femur by high-order finite element analysis validated by experimental observations. *J Biomech*. 2007;40(16):3688–3699.
- Filipov O. Epidemiology and social burden of the femoral neck fractures. *J IMAB Ann Proc*. 2014;20(4):516–518.
- Mokawem M, Bobak P, Aderinto J. The management of pertrochanteric fractures of the hip. *J Orthop Trauma*. 2012;26(2):112–123.
- Yosibash Z, Trabelsi N. Assessment of probability of bone fracture, in Provisional Application for Patent, Application number 63040549; 2020.
- Kok J, Grassi L, Gustafsson A, Isaksson H. Femoral strength and strains in sideways fall: validation of finite element models against bilateral strain measurements. *J Biomech*. 2021;122:110445.
- Falcinelli C, Schileo E, Balistreri L, et al. Multiple loading conditions analysis can improve the association between finite element bone strength estimates and proximal femur fractures: a preliminary study in elderly women. *Bone*. 2014;67:71–80.
- Badgeley MA, Zech JR, Oakden-Rayner L, et al. Deep learning predicts hip fracture using confounding patient and healthcare variables. *NPJ Digit Med*. 2019;2:31.
- Ghazikhani A, Yazdi HS, Monsefi R. Class imbalance handling using wrapper-based random oversampling. Presented at: 20th Iranian Conference on Electrical Engineering (ICEE2012), Tehran, Iran; 2012.
- Tin Kam H. Random decision forests. Presented at: Proceedings of 3rd International Conference on Document Analysis and Recognition; 1995.
- Cristianini N, Shawe-Taylor J. An introduction to support vector machines and other kernel-based learning methods. Cambridge, UK: Cambridge University Press; 2000. ν -SVM
- Crisp DJ, Burges CJC. A geometric interpretation of ν -SVM classifiers. *Adv Neural Inform Process Syst*. 2000;12:244–250.
- Ying GS, Maguire MG, Glynn RJ, Rosner B. Calculating sensitivity, specificity, and predictive values for correlated eye data. *Invest Ophthalmol Vis Sci*. 2020;61(11):29.
- Dagan N, Elnekave E, Barda N, et al. Automated opportunistic osteoporotic fracture risk assessment using computed tomography scans to aid in FRAX underutilization. *Nat Med*. 2020;26(1):77–82.
- Lenchik L, Weaver AA, Ward RJ, Boone JM, Boutin RD. Opportunistic screening for osteoporosis using computed tomography: state of the art and argument for paradigm shift. *Curr Rheumatol Rep*. 2018;20(12):74.
- Lee SJ, Anderson PA, Pickhardt PJ. Predicting future hip fractures on routine abdominal CT using opportunistic osteoporosis screening measures: a matched case-control study. *AJR Am J Roentgenol*. 2017;209(2):395–402.
- Kopperdahl DL, Aspelund T, Hoffmann PF, et al. Assessment of incident spine and hip fractures in women and men using finite element analysis of CT scans. *J Bone Miner Res*. 2014;29(3):570–580.
- Orwoll ES, Marshall LM, Nielson CM, et al. Finite element analysis of the proximal femur and hip fracture risk in older men. *J Bone Miner Res*. 2009;24(3):475–483.
- Altai Z, Qasim M, Li XS, Viceconti M. The effect of boundary and loading conditions on patient classification using finite element predicted risk of fracture. *Clin Biomech*. 2019;68:137–143.

Appendix A1

A Summary of the AFE System (Based on references^(16,19))

The femur's response under physiological loading is well described by the linear theory of elasticity, and although the bone at the macroscopic level is orthotropic, excellent predictions were obtained using isotropic inhomogeneous relations (see Yosibash and colleagues⁽²⁰⁾ for stance position loading and Altai and colleagues⁽³⁷⁾ for sideway fall loading). Thus, a linear finite element analysis was performed by Simfimi. Verification of the numerical errors was assured by monitoring the error in energy norm and the maximum and minimum principal strains at the locations of interest as the polynomial degree over the elements was increased from 1 to 6 or 8.

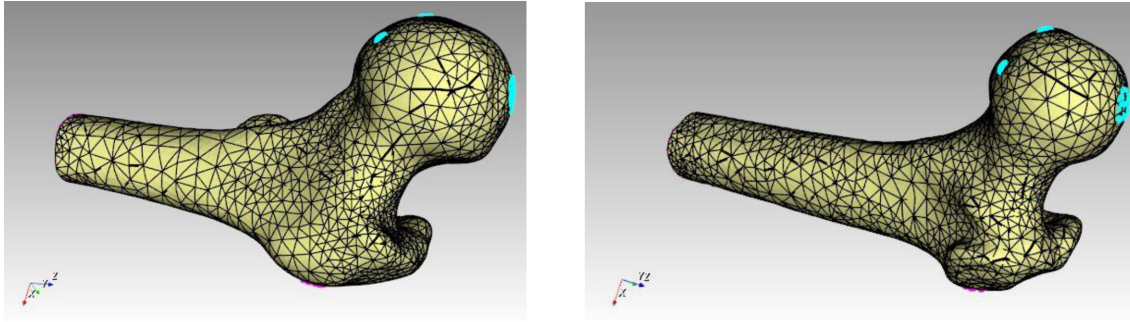


Fig. A.1. Two finite element models of the left femur of two randomly selected patients. The three locations of the applied stance, FallIN and FallP loadings on the head are shown by blue (in the web publication) and displacement boundary conditions at the lateral greater trochanter shown in pink (in the web publication).

To realize an autonomous FE analysis, several components are combined. The automatic identification of the femur's starting and ending CT slices and the femur's segmentation is obtained by a deep learning algorithm (a U-net algorithm). The U-net algorithm was trained on 178 femurs and tested on 43 femurs, resulting in a Dice score of 0.99. Another important component of the AFE is the determination of the anatomical points (center of femur's head, intercondylar notch, and center of shaft 20 mm below the lesser trochanter), for the application of the different boundary conditions.

Pointwise inhomogeneous mechanical properties are then computed at each voxel in the CT scan. The relationships between Young's modulus and ash density. These relationships are for a soft tissue CT scan with 120 KVP (as all collected CT scan) and validated by a set of experiments on fresh frozen femurs.^(21,27) for cortical and trabecular bone tissue, validated in experimental settings,⁽²⁰⁾ were used:

$$\rho_{K_2HPO_4} = 10 - 3(a \times HU + b) \quad [g/cm^3] \quad (A.1)$$

$$\rho_{ash} = 0.877 \times 1.21 \times \rho_{K_2HPO_4} + 0.08 \quad [g/cm^3] \quad (A.2)$$

$$E_{cort} = 10200 \times \rho_{ash}^{2.01} [MPa], \quad \rho_{ash} \geq 0.486 [g/cm^3] \quad (A.3)$$

$$E_{trab} = 2398 [MPa], \quad 0.3 < \rho_{ash} < 0.486 [g/cm^3] \quad (A.4)$$

$$E_{trab} = 33900 \times \rho_{ash}^{2.2} [MPa], \quad \rho_{ash} \leq 0.3 [g/cm^3] \quad (A.5)$$

These relationships are for a soft tissue CT scan with 120 KVP (as all collected CT scan) and validated by a set of experiments on fresh frozen femurs.^(21,27) Because most clinical CT scans are phantomless, a and b in (Equation A.1) are estimated by an algorithm that involves $HU = 0$ in air and a histogram of HU in the femurs, using the 0.1%

highest HU that is associated with a Young's modulus of 20 GPa (details are given in Yosibash and colleagues⁽¹⁶⁾). The Poisson ratio was set to the constant value of $\nu = 0.3$.

An automatic algorithm is applied, which generates a finite element mesh consisting of tetrahedrons having curved faces followed by an efficient high-order FE algorithm that solves the system of finite element equations and generates the data of interest. We present in Fig. A.1 two examples of femurs from two patients (which have a relatively long part of the shaft visible in the CT scan), with the three different loadings presented (stance and two fall on the side) that are solved sequentially. Each model has about 9000 to 10,000 finite elements resulting in about 900,000 degrees of freedom at $p = 6$. The entire simulation time including the pre- and postprocessing for two femurs for a patient is about 1 hour on a standard PC.

Finally, a postprocessing algorithm extracts from the finite element solutions (three different solutions that correspond

to three different boundary conditions) strains in five different anatomical locations along the femur. The maximum and minimum averaged principal strains on the bone's surface are then processed and reported in a file.